This article has been accepted for publication in IEEE Transactions on Biomedical Engineering. This is the author's version which has not been fully edited and content may change prior to final publication. Citation information: DOI 10.1109/TBME.2022.3147066

Estimation of Changes in Intracardiac Hemodynamics Using Wearable Seismocardiography and Machine Learning in Patients with Heart Failure: A Feasibility Study

Md Mobashir Hasan Shandhi*, *Member, IEEE*, Joanna Fan, J. Alex Heller, Mozziyar Etemadi, Liviu Klein† and Omer T. Inan†, *Senior Member, IEEE*

***Abstract*— *Objective:* Tracking changes in hemodynamic congestion and the consequent proactive readjustment of treatment has shown efficacy in reducing hospitalizations for patients with heart failure (HF). However, the cost-prohibitive nature of these invasive sensing systems precludes their usage in the large patient population affected by HF. The objective of this research is to estimate the changes in pulmonary artery mean pressure (PAM) and pulmonary capillary wedge pressure (PCWP) following vasodilator infusion during right heart catheterization (RHC), using changes in simultaneously recorded wearable seismocardiogram (SCG) signals captured with a small wearable patch. *Methods:* A total of 20 patients with HF (20% women, median age 55 (interquartile range (IQR), 44-64) years, ejection fraction 24 (IQR, 16-43)) were fitted with a wearable sensing patch and underwent RHC with vasodilator challenge. We divided the dataset randomly into a training–testing set ($n = 15$) and a separate validation set ($n = 5$). We developed globalized (population) regression models to estimate changes in PAM and PCWP from the changes in simultaneously recorded SCG. *Results:* The regression model estimated both pressures with good accuracies: root-mean-square-error (RMSE) of 2.5 mmHg and R^2 of 0.83 for estimating changes in PAM, and RMSE of 1.9 mmHg and R^2 of 0.93 for estimating changes in PCWP for the training-testing set, and RMSE of 2.7 mmHg and R^2 of 0.81 for estimating changes in PAM, and RMSE of 2.9 mmHg and R^2 of 0.95 for estimating changes in PCWP for the validation set respectively. *Conclusion:* Changes in wearable SCG signals may be used to track acute changes in intracardiac hemodynamics in patients with HF. *Significance:* This method holds promise in tracking longitudinal changes in hemodynamic congestion in hemodynamically-guided remote home monitoring and treatment for patients with HF.**

***Index Terms*—Cardiovascular Monitoring, Heart Failure, Hemodynamic Congestion, Right Heart Catheterization, Seismocardiogram, Wearable Sensor.**

I. Introduction

The increase in intracardiac filling pressures provides an early and actionable indication of the onset of congestion in heart failure (HF) [1]. Hemodynamic changes precede progression of chronic compensated HF to acute decompensated HF (ADHF) by several weeks [1, 2]. Recent research also shows that the product of small changes in pulmonary pressures over an extended period of time is closely associated with the transition to ADHF [2, 3]. Accordingly, tracking hemodynamics using an implantable hemodynamic congestion monitoring system and subsequent proactive HF management therapies (e.g., titration of medications, early follow-up clinic visits, etc.) to reduce subclinical congestion have demonstrated efficacy in reducing HF-related rehospitalization [4-6]. Compared to hemodynamically-guided HF management, traditional HF management therapies including tracking of daily weights, telemonitoring of vital signs and clinical symptoms to detect ADHF have not shown efficacy in reducing HF-related rehospitalization in large randomized controlled trials [7-9], as these changes occur comparatively later into the progression from compensated HF to ADHF [1].

CardioMEMS (CardioMEMS HF System, Abbott, Chicago, IL) is an example of an implantable hemodynamic monitoring system, comprising a pressure sensor implanted in the pulmonary artery (PA) [4]. Healthcare professionals receive PA pressure (PAP) readings once per day, and adjust the course of the treatment based on detection of hemodynamic congestion to keep PAP within an optimal volemic range (e.g., PA mean pressure within 10-25 mmHg) [10]. This proactive hemodynamically-guided adjustment of care has shown to decrease HF-related readmission by 37% in the randomized CHAMPION trial [4, 5], and the device received Food and Drug Administration (FDA) approval in 2014. A CardioMEMS post-approval study with 1200 HF patients has also

Research reported in this publication was supported in part by the National Heart, Lung and Blood Institute under R01HL130619. The content is solely the responsibility of the authors and does not necessarily represent the official views of the National Institutes of Health.

M. M. H. Shandhi is with the Department of Biomedical Engineering, Duke University, Durham, NC, USA. *Corresponding author email: mobashir.shandhi@duke.edu. J. Fan and L. Klein are with the Division of Cardiology, University of California San Francisco, San Francisco, CA, USA. J. A. Heller and M. Etemadi are with the School of Medicine, Northwestern University, Chicago, IL, USA. O. T. Inan is with the School of Electrical and Computer Engineering, Georgia Institute of Technology, Atlanta, GA, USA.

†Co-Senior Authors.

demonstrated a reduction in HF-related rehospitalization by 57%, comparing one-year pre-implant to one-year post-implant data from these patients [6]. The results of this PAP-guided therapeutic strategy have demonstrated efficacy in reducing not only HF-related hospitalization but also all-cause hospitalization, regardless of ejection fraction, sex, race, cause of cardiomyopathy, and presence/absence of implantable defibrillator devices or cardiac resynchronization therapy [6].

Another recently developed and tested product, remote dielectric sensing (ReDS, Sensible Medical, Netanya, Israel), tracks hemodynamic congestion indirectly (lung fluid content) via non-invasively measuring the dielectric properties of the thorax with the sensor placed on the right mid- chest and has demonstrated efficacy in reducing HF-related rehospitalization by 87% and 79% compared to pre- and post-ReDS-guided therapy in a clinical study consists of 50 patients with HF [11]. Both of these technologies (CardioMEMS and ReDS) have demonstrated the importance of tracking subclinical congestion as an early indicator of worsening HF and the efficacy of a hemodynamically-guided HF management system to reduce HF-related rehospitalization. However, high costs associated with both of the devices make them not financially feasible for the large patient population affected with HF in the US, which is roughly 6.2 million Americans [12]. For that reason, a low-cost alternative that can track changes in hemodynamic congestion has the potential to help millions of people affected by HF.

With the advent of miniaturized, inexpensive sensors, and digital health technologies, various wearable monitoring systems have been explored to monitor cardiovascular health both in healthy individuals and patients with HF. One such methodology that has demonstrated promise in monitoring cardiovascular health is seismocardiography (SCG), the local mechanical vibration of the chest wall associated with the movement of the heart and blood within the vasculature [13]. SCG timings can be used to assess changes in cardiac contractility via estimating the pre-ejection period (PEP) of the heart, with exercise and physiological perturbation [14, 15]. On top of that, SCG signals have demonstrated applications in the diagnosis and monitoring of different cardiac conditions, e.g., atrial fibrillation [16, 17], heart valve disease [18], coronary artery disease [19-21], and HF [22-24]. Importantly, recent studies have demonstrated that SCG can be used to assess the clinical status of patients with decompensated HF [23, 24]. Besides the assessment of clinical status in patients with HF, SCG has exhibited efficacy in tracking instantaneous oxygen uptake during cardiopulmonary exercise tests in patients with HF and daily life activities in healthy individuals [24, 25]. Based on these results in tracking hemodynamics with SCG for both healthy individuals and patients with HF, we hypothesized that the changes in hemodynamic congestion could be tracked with the simultaneously recorded SCG signal by estimating changes in PAP and pulmonary capillary wedge pressure (PCWP).

In this study, SCG and electrocardiogram (ECG) signals were recorded from patients with HF using a previously-validated custom-built wearable patch during right heart catheterization (RHC) [26], the gold standard of measuring hemodynamic congestion via PAP and PCWP. During the RHC procedure, the PAP and PCWP were modulated by infusing systemic vasodilators, and changes in the mean pressure values were estimated via tracking the changes in simultaneously recorded SCG signals. Various portions of the SCG signals were analyzed to understand the important segments that are providing salient information regarding changes in PAP and PCWP. Tracking acute changes in hemodynamic congestion with SCG can demonstrate the potential of using this novel wearable technology, an unobtrusive and low-cost alternative to the current monitoring systems, in longitudinal monitoring of the intracardiac filling pressures in remote HF management, and potentially ultimately reduce HF-related rehospitalization.

II. Methods

A. Experimental Protocol

The study was conducted under a protocol reviewed and approved by the University of California, San Francisco Institutional Review Boards (protocol number: 16-20442 and the date of approval: December 20, 2016). Patients were recruited from the catheterization laboratory at the University of California, San Francisco and all patients provided written consent. RHC procedures were conducted on a total of 20 HF patients (8 inpatients and 12 outpatients) who were referred for hemodynamic evaluation of their HF (patient demographics and clinical characteristics are provided in Table 1). Patients in cardiogenic shock were excluded. The dataset was separated randomly into two groups of 15 HF patients for a training-testing set and five HF patients for a separate independent validation set, with a 75:25 ratio respectively. The only constraint used to separate the dataset was to keep the same ratio of HF with reduced ejection fraction (HFrEF) and HF with preserved ejection fraction (HFpEF) subjects for both the

TABLE I
SUBJECT DEMOGRAPHICS AND CHARACTERISTICS

	All Subjects (n=20)	HFrEF Subjects (n=15)	HFpEF Subjects (n=5)	p-Value
Age, years	55 (46-64)	53 (45-62)	64 (64-66)	0.07
Sex				…
Male	16 (80%)	12 (80%)	4 (80%)	
Female	4 (20%)	3 (20%)	1 (20%)	
Height, cm	177 (168-181)	173 (168-180)	180 (175-183)	0.46
Weight, kg	93 (84-107)	92 (84-106)	93 (87-107)	0.93
BMI, kg/m^2	31 (27-33)	31 (27-33)	28 (27-33)	0.86
Ejection fraction,%	24 (16-43)	21 (16-26)	58 (58-64)	0.001
NYHA class				
I	1 (5%)	0 (0%)	1 (20%)	
II	3 (15%)	3 (20%)	0 (0%)	
III	11 (55%)	7 (47%)	4 (80%)	
IV	5 (25%)	5 (33%)	0 (0%)	
Systolic blood pressure, mmHg	115 (107-120)	110 (103-115)	120 (120-132)	0.008
Diastolic blood pressure, mmHg	68 (59-73)	70 (61-72)	64 (57-73)	0.76

Values shown are median (25th-75th percentiles) or n (% of the population) unless otherwise indicated. Statistical significance between HFrEF and HFpEF subjects in values, where applicable, was evaluated using a Mann-Whitney U test.; BMI, Body Mass Index; NYHA, New York Heart Association.

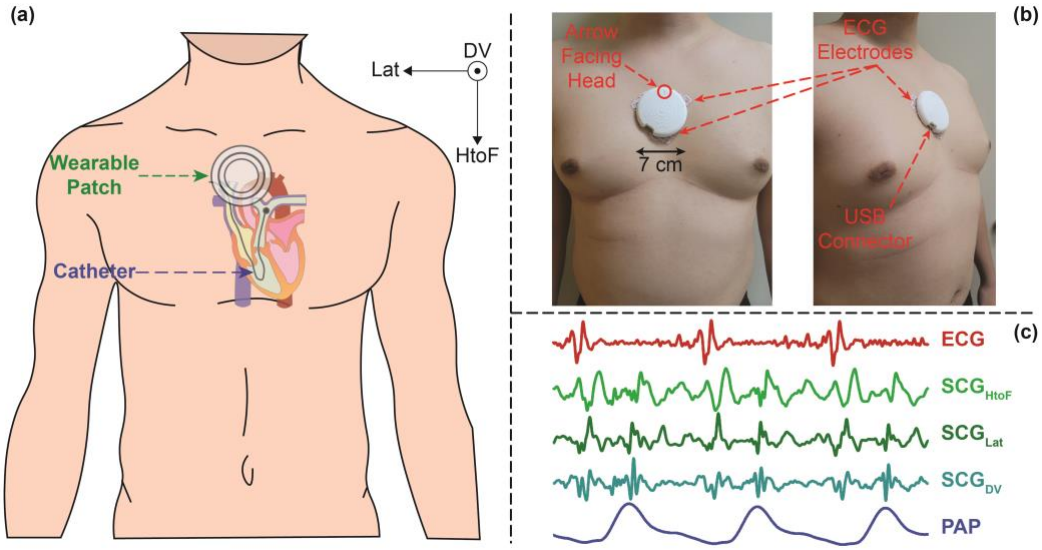

Fig. 1. (a) Experimental setup with a wearable patch placed on a subject undergoing right heart catheterization (RHC) procedure, with axes (on the upper-right) showing the axes of the seismocardiogram (SCG) signal. (b) Front (left) and side (right) view of a wearable patch placed on a representative subject. (c) Representative cardiogenic signals: electrocardiogram (ECG), triaxial SCG (head-to-foot (HtoF), lateral (Lat), and dorsoventral (DV)), and RHC pulmonary artery pressure (PAP) signal. SCG is a mechanical signal that has been associated with cardiac muscle contraction, cardiac valve movement, and movement of the blood from the left ventricle towards the aorta.

training-testing and validation set to have a dataset balance of these two HF phenotypes in both the training-testing and validation set. The random separation resulted in four HFpEF subjects in the training-testing set and one HFpEF subject in the validation set.

Fig. 1(a) and (b) illustrate the experimental setup and placement of different sensors on each patient. Before starting the RHC procedure, the custom-built wearable patch was placed just below the suprasternal notch, and the cath lab recording system was time-synchronized with the wearable patch.

The RHC procedure was carried out in a quiet, environmentally controlled cardiac catheterization laboratory with an ambient temperature of ~25°C. Right neck or right antecubital fossa regions were cleaned and prepped in a standardized sterile fashion using Chlorhexidine swabs. Local anesthesia was administered with 2% lidocaine. Under ultrasound guidance, venous access was obtained, and a 5 French (F) introducer sheath (St. Jude Medical, St. Paul, MN) was placed in the right internal jugular or right brachial vein. After at least 20 min of rest in a supine position, a 6F balloon-tipped pulmonary artery wedge catheter (Teleflex, Morrisville, NC) was advanced under fluoroscopic guidance into the right atrium, right ventricle, pulmonary arterial, and pulmonary capillary wedge positions. At each position, pressures were acquired over 60 seconds, repeated in triplicate and averaged, per standard RHC protocols [27, 28]. Cardiac output was obtained by the Fick principle and thermodilution. After baseline hemodynamics and cardiac output were measured, and after a 10 min rest in a supine position, pharmacological agents were administered at the discretion of the HF physician performing the case. Nitroglycerin was given as sublingual spray (400 or 800 mcg), and nitroprusside was administered as intravenous (IV) infusion starting at 0.3 mcg/kg/min (and titrated by 0.3 mcg/kg/min every 5 min until a hemodynamic effect was achieved). At the peak hemodynamic effect as determined by the HF physician, the hemodynamics were repeated as per baseline protocol. Thereafter, the balloon-tipped pulmonary artery wedge catheter and the venous sheath were removed. Patients were observed for adverse events following the RHC procedure and later discharged.

The wearable ECG and SCG signals were recorded continuously throughout the RHC procedure, and the timestamps from both the RHC and wearable system were used to extract the specific portions of the wearable signals later in the analysis, to estimate the changes in PAP and PCWP from the changes in wearable signals. Fig. 1(c) shows the wearable signals with corresponding PAP signal from the RHC computer during the baseline RHC recording from a representative subject.

B. Sensing Hardware

RHC pressure values were extracted from the cath lab Mac-Lab system (Mac-Lab Hemodynamic Recording System, GE Healthcare, Chicago, IL, USA) with a sampling frequency of 240 points/second. The wearable ECG and triaxial SCG (axes: head-to-foot (HtoF), dorso-ventral (DV), and lateral (Lat)) were collected, with a custom-built wearable patch as shown in Fig. 1(b), which is an improvement upon our previous version described [29]. The patch has a diameter of 7 cm and a weight of 39 gm. Initially, it samples the ECG signal at 1kHz and the SCG signals at 500 Hz and saves the data into an SD card in the patch. A custom-built graphical user interface accesses all the data into a computer and later the SCG signals were interpolated (using the 'Spline' method in Matlab R2021a) to have the same number of samples as the ECG signals. Fig. 1(c) shows representative ECG and tri-axial SCG signals from the wearable patch.

The wearable patch was synchronized with a PC. Before starting each RHC procedure, the time difference between the RHC Mac Lab PC and the wearable PC was recorded. This time

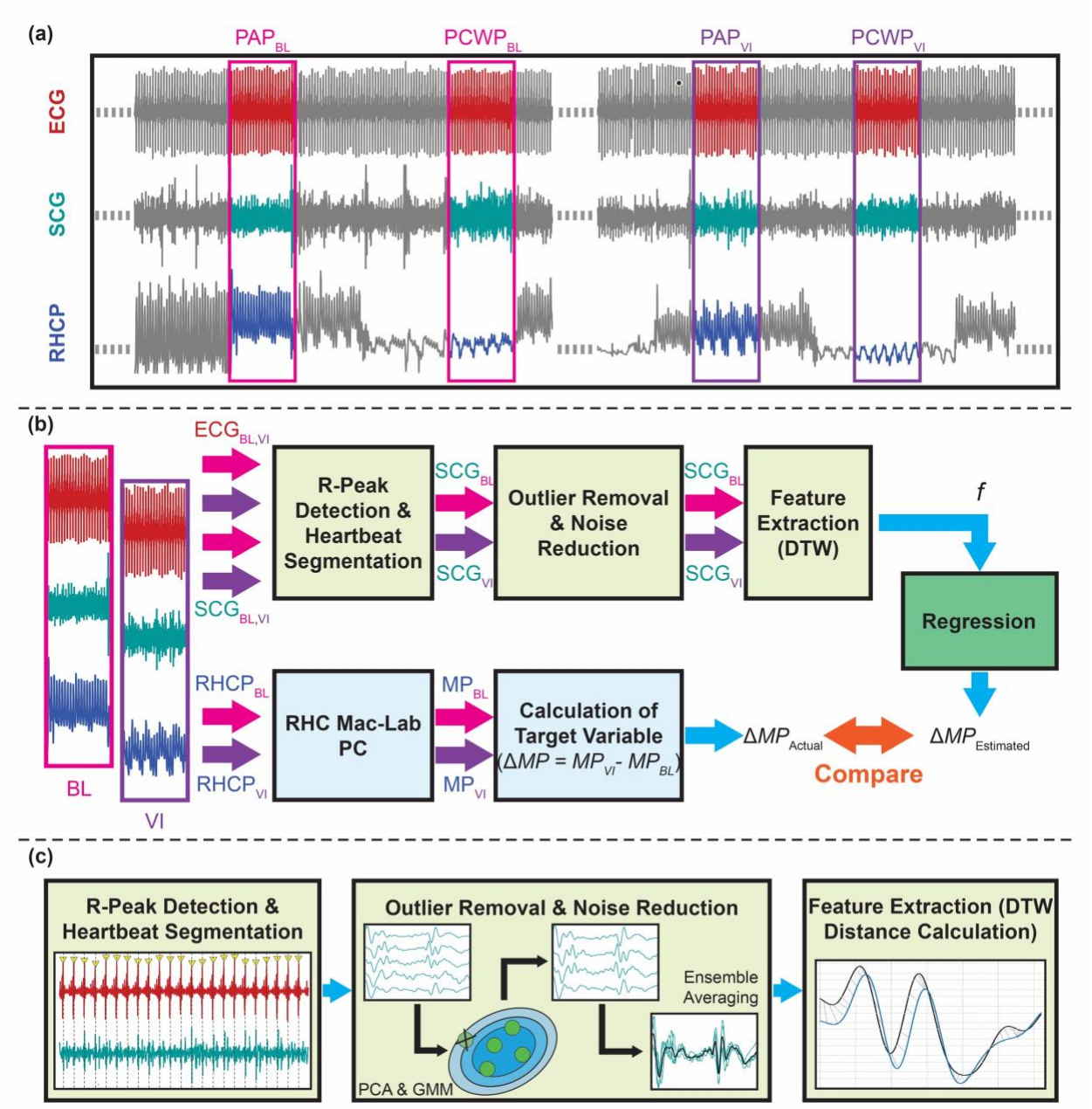

Fig. 2. Overview of the method: (a) Wearable ECG and SCG (only showing one axis of the signal for simplicity) signals were synchronized with the right heart catheterization pressure (RHCP) signal. 20s long signals from both baseline (BL) and during vasodilator infusion (VI) were extracted when the catheter was recording pulmonary artery (PA) pressure and in pulmonary capillary wedge (PCW) pressure signals. (b) The R-peaks of the ECG signal were detected and later used to segment the corresponding SCG signals into individual heartbeats. Outlier removal and noise reduction steps were performed on the SCG heartbeats, and features were extracted to be used in the regression algorithm to estimate the changes in the RHC mean pressure (MP) values (e.g., changes in pulmonary artery mean pressure (ΔPAM), and changes in pulmonary capillary wedge mean pressure (ΔPCWP)). The MP_{BL} and MP_{VI} values were extracted from the RHC Mac-Lab computer and used to calculate the target variable (ΔPAM and ΔPCWP). (c) Details on the wearable signal processing: First, the R-peaks of the ECG signals were detected, and the SCG signals were segmented into individual heartbeats. Second, SCG_{BL} and SCG_{VI} heartbeats were passed through an outlier removal algorithm (using principal component analysis [PCA] and Gaussian mixture model (GMM)) and were ensemble-averaged to have two average SCG heartbeats per axis (one for BL and one for VI). Third, dynamic time warping (DTW) distances were calculated between the BL and VI heartbeats per axes and used as features (*f*) in the regression algorithm.

difference was measured again at the end of the protocol to see if there was any significant drift between the two systems. From our experience, we have not observed any significant drift between the two systems before and after the protocol (< 1 second). During the study protocol, the clinical research coordinator (CRC) recorded the exact times of the RHC events (e.g., when the catheter was in the pulmonary artery and pulmonary capillary wedge position) using the Mac Lab PC timings. We utilized these timings plus the time difference between the wearable PC and RHC Mac Lab PC to get appropriate wearable signals corresponding to RHC pressure signals for further analysis.

C. Signal Processing and Feature Extraction

Fig. 2 illustrates the signal processing and feature extraction procedures used for the wearable signals and the pressure signal from the cath lab Mac Lab system. The PA mean pressure (PAM) and PCWP values for both the baseline (BL) and during

vasodilator infusion (VI) were extracted by a heart failure cardiologist (LK) and later used to calculate changes in PAM (ΔPAM) and changes in PCWP (ΔPCWP) by subtracting the mean pressure values during the BL from the mean pressure values during VI respectively:

$$\Delta\text{PAM} = \text{PAM}_{VI} - \text{PAM}_{BL} \quad (1)$$

$$\Delta\text{PCWP} = \text{PCWP}_{VI} - \text{PCWP}_{BL} \quad (2)$$

The PCWP_{VI} value for one subject was not recorded due to a technical issue in the Mac-Lab system and is missing from the analysis. In total, ΔPAM values were available for 20 subjects (15 subjects for the training-testing set and five subjects for the validation set), and ΔPCWP values were available for 19 subjects (14 subjects for the training-testing set and five subjects for the validation set).

For the data collection process, the physicians and attending nurses were following the standard RHC protocol [27, 28] to get PAM and PCWP values. Besides following the standard RHC protocol, they were asked to keep the catheter as stable as possible at each intra-cardiac chamber for at least 20 seconds during both BL and VI to get clean pressure signals from each chamber. The CRC recorded corresponding timestamps (from the RHC Mac Lab PC) of the start and end of the period when the clinicians confirmed the catheter was kept in a stable position in a specific intra-cardiac chamber. These timestamps were used to extract corresponding wearable ECG and SCG signals from both BL and VI states of the protocol when the catheter was at the pulmonary artery and pulmonary capillary wedge positions. The choice of 20 seconds time window to get clean pressure signals was arbitrary for this initial feasibility study without adding complexity to the standard RHC protocol. The BL and VI wearable signals were processed (filtering, removal of outliers, and ensemble averaging) separately and later used to calculate changes in the wearable signals via estimating dynamic time warping (DTW) distances [30] between the two states (BL and VI). The changes in the wearable signals were analyzed with the ΔPAM and ΔPCWP values and later used in a population regression model with leave-one-subject-out (LOSO) cross-validation on the training-testing set and later validated on the independent validation set.

1) Filtering and Heartbeat Segmentation

The raw ECG and SCG signals from the wearable patch were digitally filtered (cut-off frequencies: 0.5–40.0 Hz for the ECG and 1–40 Hz for the SCG signals) to remove out-of-band noise. These cut-off frequencies were employed to remove out-of-band noise without distorting the shape of the signals [15]. After the filtering step, a fourth SCG signal representing the accelerometer magnitude (SCG_{Mag}) was computed using vector summation of the three SCG axes already obtained (SCG_{HtoF}, SCG_{Lat}, SCG_{DV}) according to the following formula:

$$SCG_{Mag} = \sqrt{({SCG_{HtoF}}^2 + {SCG_{Lat}}^2 + {SCG_{DV}}^2)} \quad (3)$$

The ECG signal (in the 20-second frame) was amplitude-normalized and the R-peaks of the ECG signal were detected using the Pan Tompkins method [31, 32]. The SCG signals (four axes of SCG) were segmented into individual heartbeats using the R-peaks of the ECG signal. Each heartbeat was cropped to a duration of 500 ms before and after the R-peak. The 500 ms SCG frame before the R peak roughly represents the ventricular diastolic phase, and the 500 ms SCG frame after the R peak roughly represents the ventricular systolic phase of the cardiac cycle [33]. The duration of 500 ms before and after the R-peak was chosen based on our previous experience with SCG signals and generic feature extraction processes [15, 25], as most of the relevant diastolic and systolic cardiac events of interests (e.g., rapid inflow, atrial systole, isovolumetric contraction, ventricular ejection, etc.) occur within this time frame, with respect to the corresponding R-peak of ECG. A constant time window was chosen to crop the ECG and SCG signals to have a repeatable and globalized feature extraction process.

2) Outlier Removal and Ensemble Averaging

Following the heartbeat segmentation of the wearable SCG signals, the outlier heartbeats were removed from the SCG for the two distributions from the two states (BL and VI) for each axis and each portion (diastolic and systolic) of the SCG signals separately using an automated unsupervised algorithm. For outlier removal from a particular distribution, the dimension of the 500-sample long SCG heartbeats (for 500 ms long frame with a 1 kHz sampling frequency) was reduced into three dimensions by using principal component analysis (PCA) and taking the first three principal components (PC). This low-level representation of the SCG heartbeats was used in a Gaussian-mixture model (GMM) to determine the probability that each sample belongs to a particular distribution (BL or VI) for a particular portion and a particular axis of SCG. For a particular distribution, the points with the lowest 10% probability were detected as the outlier for the distribution. The cut-off of 10% was chosen based on the initial analysis, with 10%, 20%, and 30% beats removed as outliers. The number of principal components (e.g., three in this case) to create the GMM for a particular distribution was chosen based on the analysis of the percentage of variance explained by the number of PCs and tuning hyperparameters to maximize the accuracy of estimation on the training-testing set. As most of the power in the SCG signal stays in the systolic portion of the signal [13], it might end up dominating the outlier removal in the diastolic portion of the signal. For that reason, the outlier removal was performed separately for the diastolic and systolic portions of the SCG.

The actual SCG heartbeats corresponding to the outliers for the distribution were removed and resulted in two separate distributions per axis (SCG_{BL} and SCG_{VI}). The remaining heartbeats were ensemble-averaged [34] to create two ensemble-averaged heartbeats for BL and VI for a particular axis and portion, which were later used to calculate the DTW distances [30]. The ensemble-averaging step reduced the inherent variabilities and remaining noises in the SCG heartbeats. Fig. 3 shows the ensemble-averaged PAP and PCWP heartbeats from the BL and VI states and Fig. 4 shows corresponding ensemble-averaged SCG_{DV} heartbeats.

3) Dynamic Time Warping and Feature Extraction

To calculate the changes in SCG from BL to VI, we leveraged DTW and compared the DTW distances from different portions of the SCG heartbeats to the ΔPAM and ΔPCWP with correlation analyses, shown in Fig. 4. The DTW

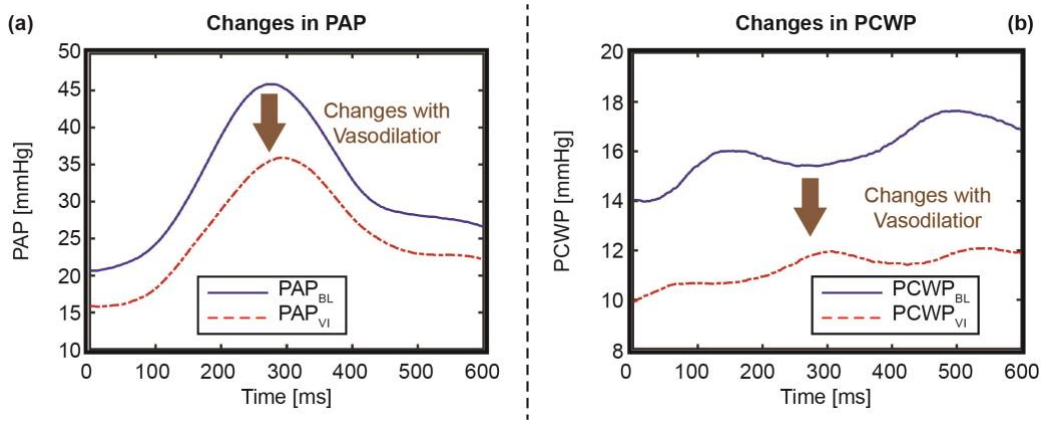

Fig. 3. Changes in (a) pulmonary artery pressure (PAP) and (b) pulmonary capillary wedge pressure (PCWP), with the infusion of vasodilator for a representative subject, with brown arrows showing the changes in the respective signals. Time "0" indicates the location of the corresponding ECG R-peak.

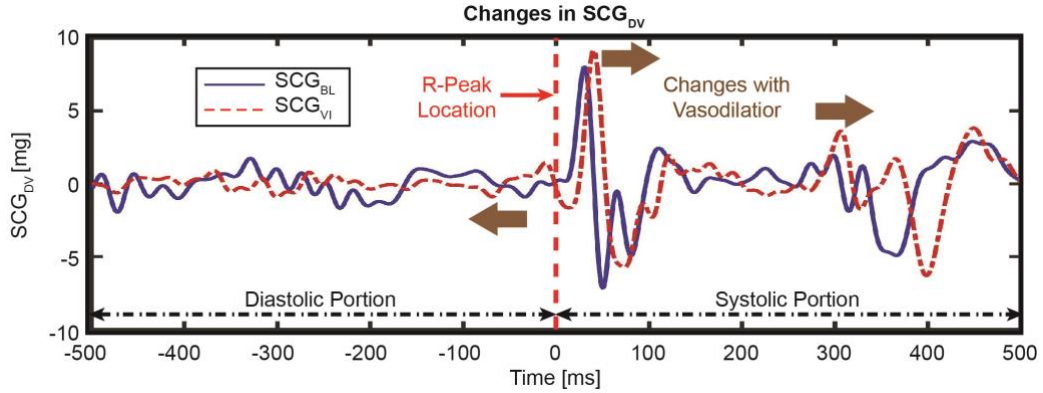

Fig. 4. Changes in SCG in the dorso-ventral direction (SCG_{DV}) with the infusion of vasodilator for a representative subject, with brown arrows showing the changes in the respective signals. Time "0" indicates the location of the corresponding ECG R-peak.

is a time-series analysis method to align signals and find similarities between signals [30]. The DTW distances between signals from BL and VI were calculated utilizing the "dtw-python" package [35] with Euclidean distance and asymmetric step patterns from different portions of the SCG heartbeats : total diastole (-500ms : R-peak), early diastole (-500ms : -200ms), late diastole (-200ms : R-peak), total systole (R-peak : 500ms), early systole (25 : 150 ms), and late systole (200 : 500ms), where negative time represents prior to the R-peak and positive time represents following the R-peak. Early diastole corresponds to the passive ventricular filling, late diastole corresponds to the atrial systole, early systole corresponds to isovolumetric contraction (IVC), and late systole corresponds to the ventricular ejection phase of the cardiac cycle.

For the DTW algorithm and feature extraction, we assumed the first and last samples are correspondent when applying the 500 ms window and the DTW distances representative of different portions in the SCG portions are corresponding to the changes in cardiac event parameters (e.g., IVC). Although, there might be some overlap between real systolic and diastolic phases of the individual heartbeats using this approach. However, we used generic time windows to approximately extracting these phases from ensemble-averaged SCG heartbeats instead of specifically extracting them from individual heartbeats using wearable ECG and SCG signals based on our prior experience with these signals [15] to mitigate the effect of inter-subject variability and motion artifacts on SCG signals.

The preprocessing and feature extraction process described above were performed in the same way for both the training-testing and validation dataset. Following the feature extraction process, only the data from the training-testing set were used to develop a regression algorithm using LOSO cross-validation. The model's hyperparameters were tuned in this step to maximize the performance (maximize the coefficients of determination, R^2, and minimize the root mean squared error, RMSE) of the developed model on the training-testing set. The resulting trained model was later validated on the independent validation set to showcase the generalizability of the developed models. The details of this step are given in the following section.

D. Regression

Before developing a regression algorithm using the data from the training-testing set, the features (i.e., DTW distances) were compared from the different portions of SCG heartbeats with the target variables (ΔPAM and ΔPCWP), using in a simple correlation analysis and the R^2 was calculated between them to analyze which segments of the SCG are more relevant to track changes in PAM and PCWP, as shown in Fig. 5.

Following the simple correlation analysis, a population level regression model with LOSO cross-validation was performed on the training-testing set to estimate the ΔPAM and ΔPCWP from the DTW distances and later validated on the independent validation set. Different regression algorithms were explored for this purpose, and, the support vector regression (SVR) [36] model was chosen as the regression model from our initial analysis.

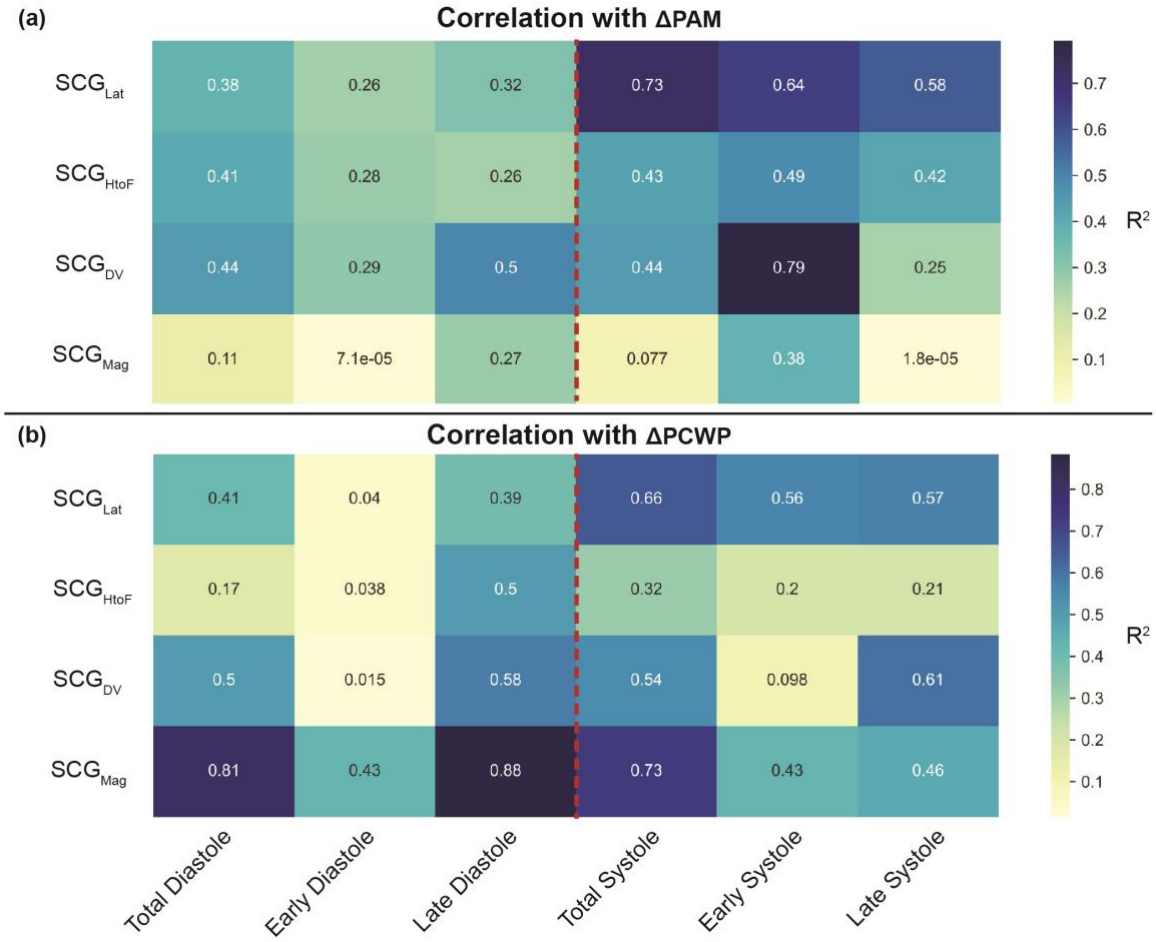

Fig. 5. Correlation analysis of the target variable (a) ΔPAM and (b) ΔPCWP with different DTW distances of corresponding SCG signals for the training-testing set, with the colorbar showing the R^2 values and the red dotted line indicating the division between ventricular diastole and systole (i.e., R-peak of corresponding ECG). Total Diastole (-500ms : R-peak), early diastole (-500ms : -200 ms), late diastole (-200ms : R-peak), total systole (R-peak : 500ms), early systole (25ms : 150ms), and late systole (200ms : 500ms).

As the simple correlation analysis between the DTW distances from different portions of the SCG heartbeats and corresponding target variables (ΔPAM and ΔPCWP) for the training-testing set is shown in Fig. 5, not all the changes from the different portions of the SCG (i.e., DTW distances) are relevant to the changes in the mean pressures (MP). For that reason, a feature selection technique was performed using a sequential forward selection (SFS) algorithm [37] to select the top five features as the estimating variables in the regression model using a linear SVR regressor.

Following the feature selection, we performed a grid search to tune hyperparameters (kernel, C, gamma, coef0, etc.) of the SVR regressor [38] to maximize the accuracy of estimation using a LOSO cross-validation for 15 subjects in the training-testing set. This grid search method resulted in two hyperparameter-tuned models: one for the estimation of ΔPAM (SVR with a sigmoid kernel, C=3, gamma='auto', coef0=0.5) and one for the estimation of ΔPCWP (SVR with a linear kernel, C=3, gamma='auto', coef0=0.0001). This grid search with cross-validation method was used to develop a global regression model with optimized hyperparameters on the data in the training–testing set only. Following the grid search, we used the hyperparameter tuned SVR regression model on the selected (using SFS method) DTW distances to estimate the target variables in the training-testing set using a LOSO cross-validation, training the model using data from 14 subjects and leaving one subject out at each fold. The target variables (ΔPAM and ΔPCWP) were predicted for the left-out subject, repeating these 14 more times with a different subject excluded each time. As a result, we obtained predictions for all 15 subjects in the training-testing set. For the validation of the global model, the regression model (with the optimized hyperparameters) was trained on the whole training–testing set (data from 15 subjects) and tested on the separate validation set (data from 5 subjects). As a result, all the target variables were predicted, from all 20 subjects.

Four figures of merit that are commonly used in the existing literature were used to evaluate the regression model and approach. First, the RMSE was calculated between the estimated target variable (ΔMP_{Pred}) and the ground truth target variable from the Mac-Lab system (ΔMP_{Act}):

$$RMSE = \sqrt{\frac{1}{N}\sum_{i=1}^{N}(\Delta MP_{Pred} - \Delta MP_{Act})^2} \quad (4)$$

Second, the normalized RMSE (NRMSE) was calculated:

$$NRMSE = \frac{RMSE}{|\frac{1}{N}\sum_{i=1}^{N}\Delta MP_{Act}|} \times 100 \quad (5)$$

Third, a simple correlation analysis (Pearson) was performed between the true values and the predictions of ΔMP to get the statistical significance of prediction, and the R^2 between the true and predicted values was calculated. In this work, p-values below 0.05 were considered to be statistically significant.

Fourth, Bland-Altman analysis was performed between the true values and the predictions of ΔMP to get the limit of agreement (LOA) (i.e., 1.96 X standard deviation of the mean difference between the true values and the predictions). The RMSE, R^2, and LOA values were calculated for the training-testing set and the validation set separately.

III. Results

Patient demographics and clinical characteristics are detailed in Table 1, and RHC characteristics are provided in Table 2. There were 15 patients with HFrEF and 5 with HFpEF; four patients were women, and the median age was 55 (interquartile range, IQR, 46-64) years. The median weight was 93 (IQR, 84-107) kg, the median height was 177 (IQR, 168-181) cm, and the median ejection fraction (EF) was 24 (IQR, 16-43).

With vasodilator infusion, the PAM and PCWP decreased by a median of 8.5 (IQR, 4.5-13.25) mmHg and 6 (IQR, 3-11.25) mmHg, respectively, from the corresponding BL values. Fig. 3 and 4 show the changes in PAP and PCWP signals and the changes in SCG_{DV} with vasodilator infusion for one representative subject. Note that all the signals shown in both the figures are synchronized with the corresponding R-peak. The overall mean of the PAP and PCWP signals decreased with vasodilator infusion, whereas the systolic portion of the SCG_{DV} signal shifted later with respect to the ECG R-peak following vasodilator infusion.

Fig. 5 shows the R^2 values between the dynamic time warping (DTW) distances from different portions and axes of the SCG signals with ΔPAM and ΔPCWP for the training-testing set. In the case of ΔPAM, the changes in SCG during the early systole (isovolumetric contraction, IVC, period) provided the most relevant information related to changes in the PAM, with changes in SCG in the dorso-ventral direction (SCG_{DV}) during the IVC period showing the highest R^2 of 0.79 with ΔPAM. In the case of ΔPCWP, the changes in the SCG during the late diastole (atrial systole) phase provided the most relevant information related to changes in PCWP, with changes in SCG magnitude signal (SCG_{Mag}) during the late diastole period (atrial systole) showing the highest R^2 of 0.88 with ΔPCWP.

Fig. 6 and 7 show the correlation analysis and Bland-Altman analysis between the actual (measured) and the estimated ΔPAM and ΔPCWP values for both the training-testing and validation set, respectively. The results show an RMSE of 2.5 mmHg, an NRMSE of 28%, an R^2 of 0.83, and an LOA of 5 mmHg for the training-testing set and an RMSE of 2.7 mmHg, an NRMSE of 33%, an R^2 of 0.81, and an LOA of 3.8 mmHg for the validation set for ΔPAM, and an RMSE of 1.85 mmHg, an NRMSE of 23%, an R^2 of 0.93, and an LOA of 4.6 mmHg for the training-testing set and an RMSE of 2.9 mmHg, an NRMSE of 38%, an R^2 of 0.95, and an LOA of 6.4 mmHg for the validation set for ΔPCWP.

Fig. 8 shows the selected five DTW distances using the feature selection technique (SFS algorithm) mentioned in the method section, and their relative importance (weights) in the regression model (SVR with a linear kernel) for the estimation of ΔPAM and ΔPCWP in the training-testing set, with the top feature related to ΔPAM being the change SCG_{Lat} during the IVC period and the top feature related to ΔPCWP being the change in SCG_{Lat}. Similar to the results obtained from the individual correlation analysis (in Fig. 5) between the target variables (ΔPAM and ΔPCWP) with the DTW distances, four of the top five features for the ΔPAM are from the systolic portion of the SCG, and one is from the diastolic portion of the SCG. In the case of ΔPCWP, four of the top five are from the systolic portion of the SCG, and one is from the diastolic portion of the SCG.

IV. Discussion

This work shows that changes in SCG may track acute changes in PAM and PCWP due to systemic vasodilator infusion in patients with HF. Although the LOA values between the true and estimated values are relatively high, the reported RMSE, NRMSE, and R^2 values show the feasibility and

TABLE 2
RIGHT HEART CATHETERIZATION RESPONSES

	All Subjects (n=20)			Training-Testing Set Subjects (n=15)			Validation Set Subjects (n=5)		
	BL	VI	p-Value	BL	VI	p-Value	BL	VI	p-Value
PAMP, mmHg	34 (32-37)	26 (24-28)	<0.001	35 (31-38)	26 (24-28)	<0.001	33 (32-34)	26 (24-28)	0.062
PCWP, mmHg	22 (18-25)	13 (12-17)*	<0.001	21 (18-26)	14 (10-18)*	<0.001	22 (21-24)	13 (13-16)	0.062
HR_PA, BPM	82 (69-94)	85 (69-93)*	0.736	82 (70-94)	89 (70-94)	0.68	70 (67-88)	72 (67-92)	1
HR_PCW, BPM	80 (69-90)	79 (69-90)	0.42	80 (67-90)	78 (69-89)*	0.328	87 (72-89)	88 (75-90)	0.5625
RAMP, mmHg	9 (7-13)	7 (5-11)*	0.002	9 (6-14)	7 (5-11)*	0.008	10 (9-13)	7 (6-7)*	0.5
SV, mL/beat	47 (40-65)*	65 (47-75)*	0.059	46 (39-61)*	60 (48-80)*	0.03	59 (43-68)	66 (46-68)	1
Fick CO, L/min	3.8 (3.4-4.6)*	4.6 (4-5.3)*	0.01	3.8 (3.3-4.3)*	4.5 (4-5.5)*	0.045	4.1 (3.5-4.7)	4.6 (4-4.9)	0.25
Thermodilution CO, L/min	3.7 (3.3-4.4)*	4.6 (3.7-5.6)*	0.002	3.5 (3.3-4.4)	4.6 (3.7-5.8)*	0.007	3.9 (3.5-4.2)*	4.1 (3.7-4.9)	0.25
CI, L/min/m^2	1.8 (1.7-2)	2.1 (1.9-2.7)*	<0.001	1.8 (1.7-2)	2.2 (1.9-2.7)*	0.002	1.9 (1.7-2)	2.1 (2.1-2.2)	0.188

*Missing values for one or more subjects.

Values shown are median (25th-75th percentiles) unless otherwise indicated. Statistical significance between BL and VI periods in values, where applicable, was evaluated using a Wilcoxon signed rank test. BL, Baseline Values; VI, Vasodilator Infused values, PAMP, Pulmonary Artery Mean Pressure, PCWP, Pulmonary Capillary Wedge Pressure, RAMP, Right Atrial Mean Pressure, SV, Stroke Volume, CO, Cardiac Output, CI, Cardiac Index.

This article has been accepted for publication in IEEE Transactions on Biomedical Engineering. This is the author's version which has not been fully edited and content may change prior to final publication. Citation information: DOI 10.1109/TBME.2022.3147066

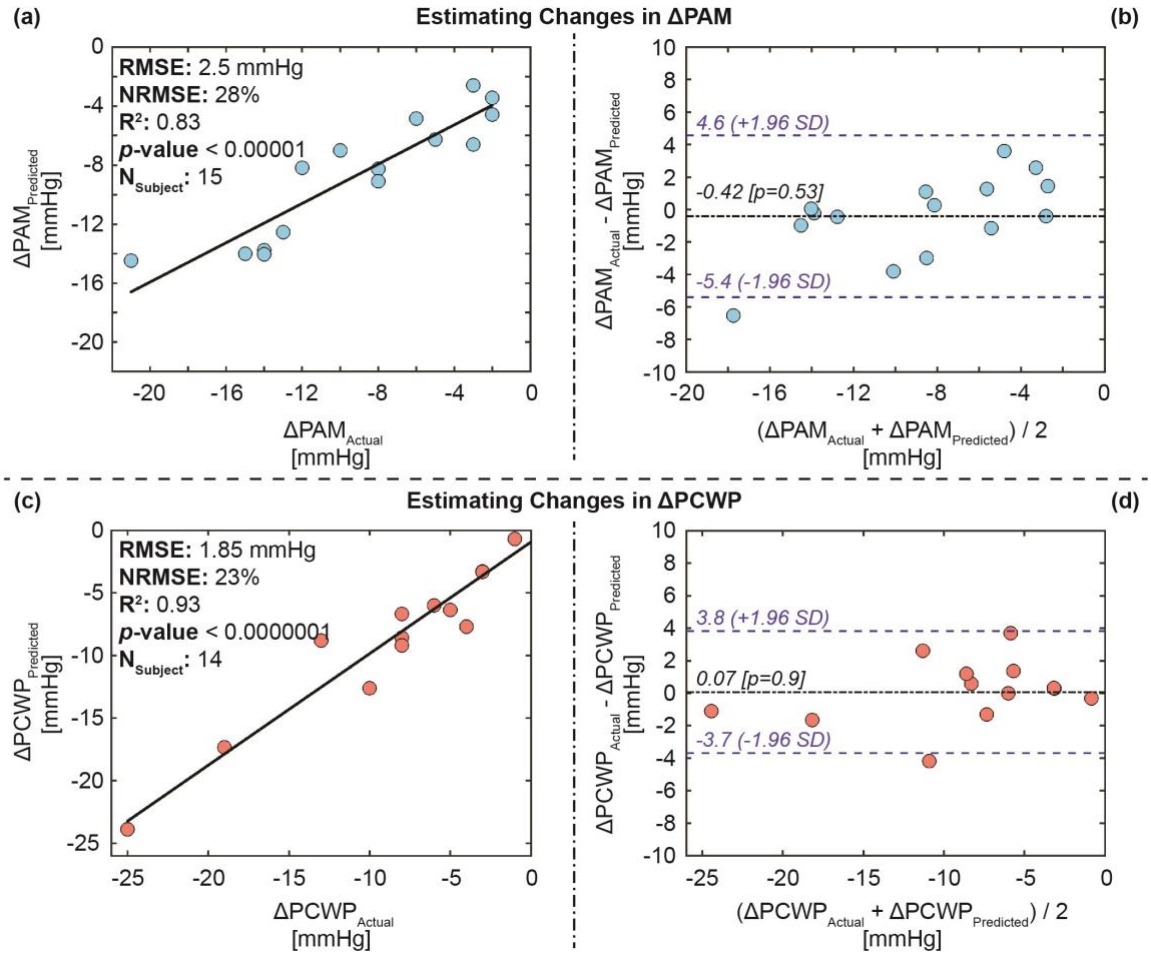

Fig. 6. Estimation results for the training-testing set: (a) Correlation analysis for ΔPAM predicted vs. ΔPAM actual, (b) Bland-Altman analysis for ΔPAM predicted and ΔPAM actual, (c) correlation analysis for ΔPCWP predicted vs. ΔPCWP actual, and (d) Bland-Altman analysis for ΔPCWP predicted and ΔPCWP actual. In the Bland-Altman plots, the black line indicates the mean, while the blue dashed lines indicate mean ± 1.96 x standard deviation (SD).

potential of this technology in estimating changes in intracardiac hemodynamics. Future studies with a larger population and more complex algorithms should improve the accuracy of estimation even further. The results from this initial feasibility study suggest that SCG signals obtained using a wearable patch can potentially track changes in hemodynamic congestion in future studies. These promising initial results provide a foundation for tracking changes in hemodynamics in patients with HF in their daily life and activities via wearable sensors. With further research, this approach could enable longitudinal remote monitoring of hemodynamic congestion, which could potentially enable a low-cost alternative to the already proven hemodynamically-guided remote HF management using CardioMEMS or ReDS systems, and one that could be applied to a broader population of patients with HF.

Two important findings in this work were the individual feature (DTW distances) correlation and feature importance ranking corresponding to the changes in PAM and PCWP due to systemic vasodilator infusion. The results from this work show that the changes in SCG during the ventricular systolic portion of the cardiac cycle provide salient information about the changes in PAM, whereas the changes in the SCG signals during atrial systole (active ventricular diastolic period) provided the most pertinent information regarding changes in PCWP. It might be explained with physiological rationale, as the pulmonary artery is directly connected to the right ventricle, the ventricular systole (contraction) phase is dominating the changes in PAM. On the other hand, the pulmonary capillaries are connected to the left atrium and showing more relation with atrial systole. These preliminary results should be verified with simultaneous imaging modalities in a large population study with diversified subjects with various cardiovascular conditions.

With vasodilator infusion, the PAM and PCWP decrease as does preload (as observed as the decrease in RAMP), and IVC time interval (i.e., PEP) is inversely correlated with preload [39]. For that reason, with a decrease in preload, we observe an increase in PEP (as shown in Fig. 4), which is expected. These scientific findings pave the way toward elucidating the origin of the SCG signal itself, and inform the use of these signals to extract physiologically meaningful information beyond vital signs and cardiac timing intervals as have previously been demonstrated. These results also show the importance of the ventricular diastolic portion of the SCG signals, which is often neglected in most research works focused on SCG [13, 40]. Future studies should incorporate imaging modalities to understand how the changes in SCG are related to underlying physiological changes due to physiological or pharmacological perturbation.

Another important finding from this work is the use of simple linear models (linear SVR) rather than complex non-linear

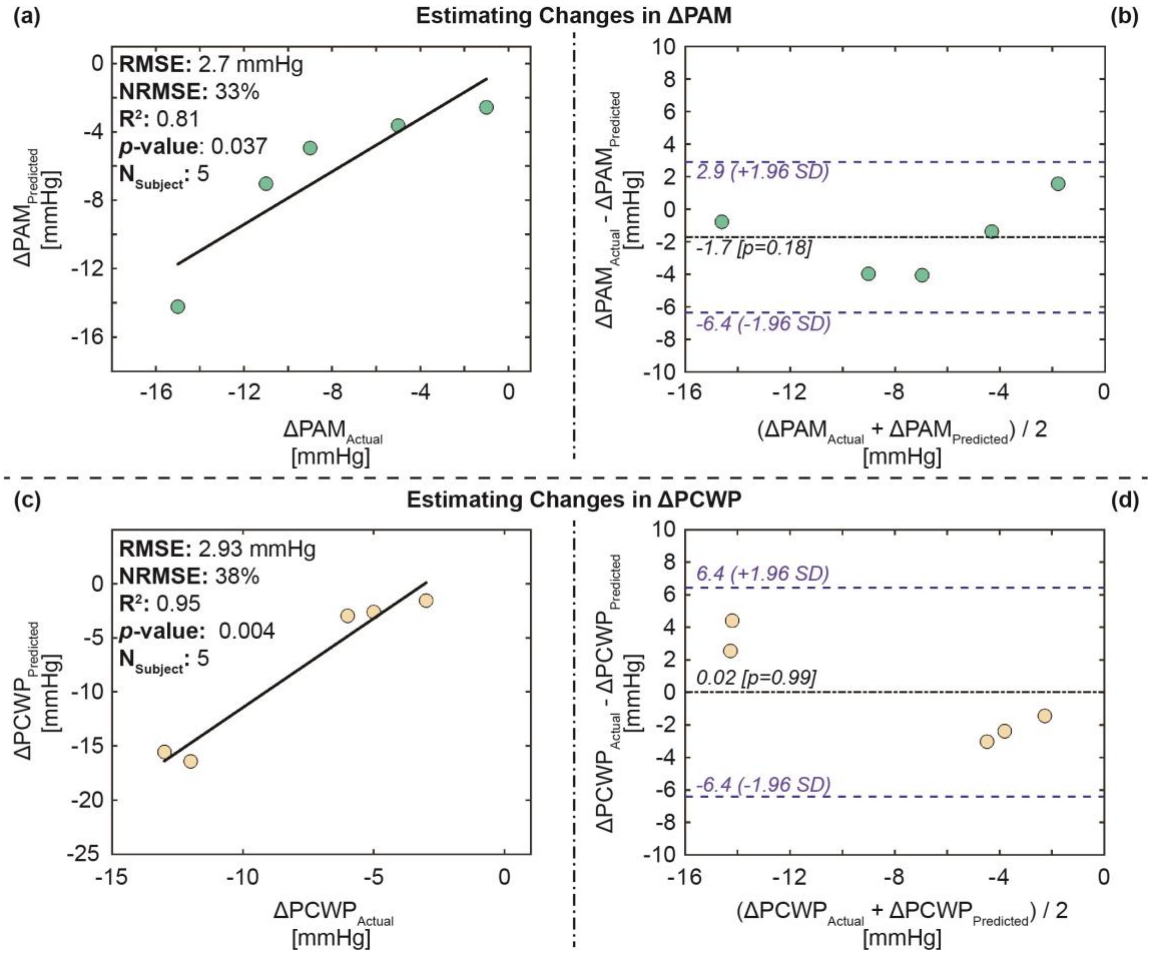

Fig. 7. Estimation results for the validation set: (a) Correlation analysis for ΔPAM predicted vs. ΔPAM actual, (b) Bland-Altman analysis for ΔPAM predicted and ΔPAM actual, (c) correlation analysis for ΔPCWP predicted vs. ΔPCWP actual, and (d) Bland-Altman analysis for ΔPCWP predicted and ΔPCWP actual. In the Bland-Altman plots, the black line indicates the mean, while the blue dashed lines indicate mean ± 1.96 x standard deviation (SD).

models to estimate the changes in hemodynamic congestion. Simple linear models can provide more insights into the model and corresponding features used to build the model compared to the complex non-linear models, which are sometimes "black box" in nature. As there was a small number of subjects for this study, using a simpler regression model provided a better understanding of the important features (segments and axes of the SCG) that are relevant to acute changes in hemodynamic congestion, and increased confidence in the generalizability of the methods. These methods make the models more physiologically insightful and interpretable. Nevertheless, this is a feasibility study, and the results from this initial study should be verified with a larger population study to validate these initial results.

Another key finding of this study was the use of noise reduction and outlier removal that improved the overall accuracy of estimation significantly. The results from the analysis demonstrated that having 20-30 seconds of high-quality wearable ECG and SCG recordings is sufficient to track changes in hemodynamic congestion. However, this study was carried out in a controlled clinical environment with trained professionals, and thus in home monitoring settings, longer recording times may be needed. The choice of 20 seconds time window to get clean pressure signals was arbitrary for this initial feasibility study without adding complexity to the standard RHC protocol. Future work should further validate and expand this methodology to see the minimum length of the data needed to estimate changes in PAM and PCWP from wearable SCG and ECG signals from a wide variety of window lengths.

Our previous work with the same wearable patch demonstrated that cardiopulmonary fitness parameters (i.e., instantaneous oxygen uptake and clinical state of patients) can be tracked from both patients with HF in a controlled clinical setting (cardiopulmonary exercise test) and healthy subjects in an uncontrolled daily life setting [24, 25]. Incorporating the method of tracking changes in hemodynamic congestion using SCG described in this paper with the methods of tracking cardiopulmonary parameters using SCG in our previous work [24, 25] should be leveraged in future work.

Though this feasibility study has shown promise in tracking changes in PAM and PCWP in patients with HF, it has multiple limitations. This study was conducted with 20 subjects, including both patients with HFrEF and HFpEF. However, the pathophysiology of the two HF subgroups may present different relationships between the changes in SCG with changes in PAM and PCWP. Due to the small number of subjects for this preliminary study, it was not possible to analyze such phenotypic differences. Future studies should verify the analysis of this study in a large patient population with HF, with emphasis on the differences between the subgroups. Another

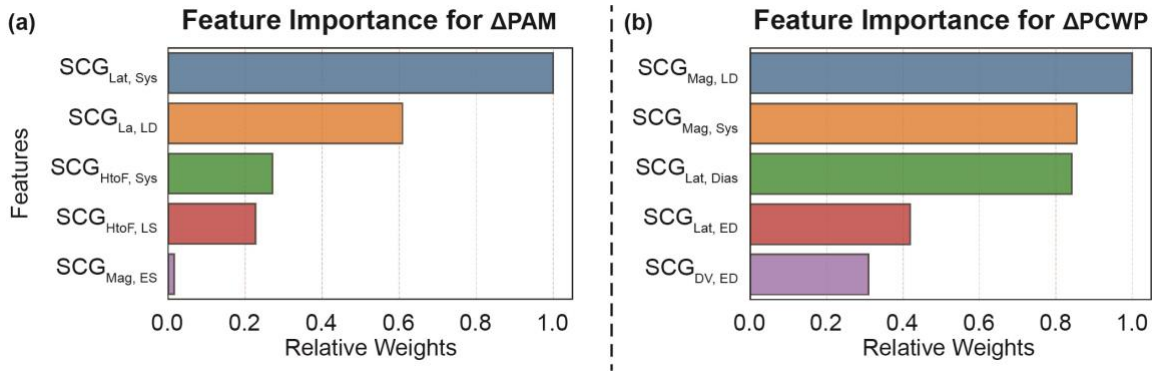

Fig. 8. Relative feature importance ranking (i.e., relative weights) of the features in the regression algorithm for (a) ΔPAM and (b) ΔPCWP on the training-testing set. Dias: Total Diastole, ED: Early Diastole, LD: Late Diastole, Sys: Systole, ES: Early Systole, and LS: Late Systole. Time-length for the segments is explained in the Fig. 5.

limitation is that this study has estimated changes in PAM and PCWP only. Future studies should look into changes in other key variables from the RHC procedure, e.g., right atrial pressure, right ventricular pressure, stroke volume, and cardiac output.

For this study, 500 ms of SCG heartbeats after and before corresponding ECG R-peaks were considered as representative for the systolic and diastolic portions of the cardiac cycle. However, there might be some overlap between the real systolic and diastolic phases using this approach due to heart rate variability in the individual heartbeats. It could be mitigated via identifying the real systolic and diastolic portions of the individual heartbeats by identifying aortic/mitral valve opening and closing points from simultaneously recorded wearable ECG and SCG signals. Although researchers explored different approaches to identify aortic/mitral valve opening and closing points from simultaneously recorded wearable ECG and SCG signals [41-46], the generalizability of these approaches remains questionable due to high inter-subject variability in SCG [15]. For example, our previous work demonstrates that general time-domain feature extraction of SCG and advanced machine learning regression algorithms can perform significantly well (p-value < 0.05) in estimating changes in the PEP of the heart due to exercise compared to the traditional method of utilizing SCG characteristic points to estimate PEP via identifying aortic valve opening points [15]. Besides, ensemble averaging of SCG heartbeats also helps to improve the signal-to-noise ratio and reduce beat-to-beat variation of the signals which can further impact the reliable feature extraction from SCG due to high inter-subject variability and motion artifacts. For these reasons, we chose generic feature extraction from the ensemble-averaged SCG heartbeats with some domain knowledge to extract approximate systolic and diastolic portions of the SCG heartbeat instead of specifically isolating systolic and diastolic portions of the individual SCG heartbeats. Future work should explore if identifying the real systolic and diastolic phases of the individual heartbeats from wearable ECG and SCG signals improves the estimation accuracy even further.

In this study, the change in hemodynamic congestion with vasodilator infusion was considered only. Future studies should include other pharmacological agents, e.g., diuretics, beta-blocker, angiotensin receptor blockers - neprilysin inhibitors, and verify whether changes in simultaneously recorded SCG can be used to track changes due to other pharmacological agents as well. Also, data were collected during the RHC procedure in a controlled clinical environment for acute changes in hemodynamic congestion. To be a reliable sensor for outpatient HF management, the device and the methods should be verified with longitudinal remote home hemodynamic congestion monitoring systems (e.g., CardioMEMS). Future studies should also focus on how motion artifacts impact estimation accuracy.

V. Conclusion

In this work, we have estimated the changes in pulmonary artery mean pressure and pulmonary capillary wedge pressure in patients with HF due to vasodilator infusion with the changes in simultaneously recorded SCG signal. We have developed a global regression model for the estimation of ΔPAM and ΔPCWP using machine learning algorithms validated with leave-one-subject-out cross-validation. We have demonstrated that tracking changes in SCG may track changes in the subclinical congestion, which has the potential to be used for remote home management for patients with HF. Overall, this work demonstrates the capability of an unobtrusive wearable patch to track hemodynamic congestion. Success in this regard represents a considerable step towards the hemodynamically-guided affordable HF management for the larger population affected by HF.

VI. Disclosures

OTI is a co-founder, Board member, and Chief Scientific Advisor for Cardiosense, a company focused on developing wearable SCG sensing hardware and algorithms for remote heart failure management.

References

[1] P. B. Adamson, "Pathophysiology of the transition from chronic compensated and acute decompensated heart failure: new insights from continuous monitoring devices," *Current heart failure reports,* vol. 6, no. 4, p. 287, 2009.

[2] M. R. Zile *et al.*, "Hemodynamic factors associated with acute decompensated heart failure: part 1—insights into pathophysiology," *Journal of cardiac failure,* vol. 17, no. 4, pp. 282-291, 2011.

[3] P. B. Adamson *et al.*, "Hemodynamic factors associated with acute decompensated heart failure: part 2—use in automated detection," *Journal of cardiac failure,* vol. 17, no. 5, pp. 366-373, 2011.

[4] W. T. Abraham *et al.*, "Wireless pulmonary artery haemodynamic monitoring in chronic heart failure: a randomised controlled trial," *The Lancet,* vol. 377, no. 9766, pp. 658-666, 2011.

[5] W. T. Abraham *et al.*, "Sustained efficacy of pulmonary artery pressure to guide adjustment of chronic heart failure therapy: complete follow-up results from the CHAMPION randomised trial," *The Lancet*, vol. 387, no. 10017, pp. 453-461, 2016.

[6] D. M. Shavelle *et al.*, "Lower Rates of Heart Failure and All-Cause Hospitalizations During Pulmonary Artery Pressure-Guided Therapy for Ambulatory Heart Failure: One-Year Outcomes From the CardioMEMS Post-Approval Study," *Circulation: Heart Failure*, vol. 13, no. 8, p. e006863, 2020. [Online]. Available: https://www.ahajournals.org/doi/pdf/10.1161/CIRCHEARTFAILURE.119.006863?download=true.

[7] R. C. Bourge *et al.*, "Randomized controlled trial of an implantable continuous hemodynamic monitor in patients with advanced heart failure: the COMPASS-HF study," *Journal of the American College of Cardiology*, vol. 51, no. 11, pp. 1073-1079, 2008.

[8] S. I. Chaudhry *et al.*, "Telemonitoring in patients with heart failure," *New England Journal of Medicine*, vol. 363, no. 24, pp. 2301-2309, 2010.

[9] M. K. Ong *et al.*, "Effectiveness of remote patient monitoring after discharge of hospitalized patients with heart failure: the better effectiveness after transition–heart failure (BEAT-HF) randomized clinical trial," *JAMA internal medicine*, vol. 176, no. 3, pp. 310-318, 2016.

[10] P. B. Adamson *et al.*, "CHAMPION trial rationale and design: the long-term safety and clinical efficacy of a wireless pulmonary artery pressure monitoring system," *Journal of cardiac failure*, vol. 17, no. 1, pp. 3-10, 2011.

[11] O. Amir *et al.*, "Evaluation of remote dielectric sensing (ReDS) technology-guided therapy for decreasing heart failure re-hospitalizations," *International journal of cardiology*, vol. 240, pp. 279-284, 2017.

[12] E. J. Benjamin *et al.*, "Heart disease and stroke Statistics-2019 update a report from the American Heart Association," *Circulation*, 2019.

[13] O. T. Inan *et al.*, "Ballistocardiography and seismocardiography: A review of recent advances," *IEEE journal of biomedical and health informatics*, vol. 19, no. 4, pp. 1414-1427, 2014. [Online]. Available: https://ieeexplore.ieee.org/document/6916998/.

[14] A. Q. Javaid, N. F. Fesmire, M. A. Weitnauer, and O. T. Inan, "Towards robust estimation of systolic time intervals using head-to-foot and dorso-ventral components of sternal acceleration signals," in *2015 IEEE 12th international conference on wearable and implantable body sensor networks (BSN)*, 2015: IEEE, pp. 1-5.

[15] M. M. H. Shandhi, B. Semiz, S. Hersek, N. Goller, F. Ayazi, and O. T. Inan, "Performance analysis of gyroscope and accelerometer sensors for seismocardiography-based wearable pre-ejection period estimation," *IEEE journal of biomedical and health informatics*, vol. 23, no. 6, pp. 2365-2374, 2019. [Online]. Available: https://ieeexplore.ieee.org/document/8627923/.

[16] T. Hurnanen *et al.*, "Automated detection of atrial fibrillation based on time–frequency analysis of seismocardiograms," *IEEE journal of biomedical and health informatics*, vol. 21, no. 5, pp. 1233-1241, 2016.

[17] O. Lahdenoja *et al.*, "Atrial fibrillation detection via accelerometer and gyroscope of a smartphone," *IEEE Journal of Biomedical and Health Informatics*, vol. 22, no. 1, pp. 108-118, 2017.

[18] C. Yang, B. Ojha, N. D. Aranoff, P. Green, and N. Tavassolian, "Classification of Aortic Stenosis Before and After Transcatheter Aortic Valve Replacement Using Cardio-mechanical Modalities," in *2020 42nd Annual International Conference of the IEEE Engineering in Medicine & Biology Society (EMBC)*, 2020: IEEE, pp. 2820-2823.

[19] Z. Iftikhar *et al.*, "Multiclass classifier based cardiovascular condition detection using smartphone mechanocardiography," *Scientific reports*, vol. 8, no. 1, pp. 1-14, 2018.

[20] K. Pandia, O. T. Inan, G. T. Kovacs, and L. Giovangrandi, "Extracting respiratory information from seismocardiogram signals acquired on the chest using a miniature accelerometer," *Physiological measurement*, vol. 33, no. 10, p. 1643, 2012.

[21] D. M. Salerno and J. Zanetti, "Seismocardiography for monitoring changes in left ventricular function during ischemia," *Chest*, vol. 100, no. 4, pp. 991-993, 1991.

[22] A. Q. Javaid *et al.*, "Quantification of posture induced changes in wearable seismocardiogram signals for heart failure patients," in *2016 Computing in Cardiology Conference (CinC)*, 2016: IEEE, pp. 777-780.

[23] O. T. Inan *et al.*, "Novel wearable seismocardiography and machine learning algorithms can assess clinical status of heart failure patients," *Circulation: Heart Failure*, vol. 11, no. 1, p. e004313, 2018. [Online]. Available: https://www.ahajournals.org/doi/pdf/10.1161/CIRCHEARTFAILURE.117.004313?download=true.

[24] M. M. H. Shandhi *et al.*, "Wearable Patch Based Estimation of Oxygen Uptake and Assessment of Clinical Status during Cardiopulmonary Exercise Testing in Patients with Heart Failure," *Journal of Cardiac Failure*, 2020.

[25] M. M. H. Shandhi *et al.*, "Estimation of Instantaneous Oxygen Uptake during Exercise and Daily Activities using a Wearable Cardio-Electromechanical and Environmental Sensor," *IEEE Journal of Biomedical and Health Informatics*, 2020.

[26] G. M. Kubiak, A. Ciarka, M. Biniecka, and P. Ceranowicz, "Right heart catheterization—Background, physiological basics, and clinical implications," *Journal of clinical medicine*, vol. 8, no. 9, p. 1331, 2019.

[27] E. L. Bonno, M. C. Viray, G. R. Jackson, B. A. Houston, and R. J. Tedford, "Modern Right Heart Catheterization: Beyond Simple Hemodynamics," *Advances in Pulmonary Hypertension*, vol. 19, no. 1, pp. 6-15, 2020.

[28] P. Sorajja *et al.*, "SCAI/HFSA clinical expert consensus document on the use of invasive hemodynamics for the diagnosis and management of cardiovascular disease," *Catheterization and cardiovascular interventions: official journal of the Society for Cardiac Angiography & Interventions*, vol. 89, no. 7, pp. E233-E247, 2017.

[29] M. Etemadi, O. T. Inan, J. A. Heller, S. Hersek, L. Klein, and S. Roy, "A wearable patch to enable long-term monitoring of environmental, activity and hemodynamics variables," *IEEE transactions on biomedical circuits and systems*, vol. 10, no. 2, pp. 280-288, 2016.

[30] H. Sakoe and S. Chiba, "Dynamic programming algorithm optimization for spoken word recognition," *IEEE transactions on acoustics, speech, and signal processing*, vol. 26, no. 1, pp. 43-49, 1978.

[31] A. L. Goldberger *et al.*, "PhysioBank, PhysioToolkit, and PhysioNet: components of a new research resource for complex physiologic signals," *circulation*, vol. 101, no. 23, pp. e215-e220, 2000.

[32] J. Pan and W. J. Tompkins, "A real-time QRS detection algorithm," *IEEE transactions on biomedical engineering*, no. 3, pp. 230-236, 1985.

[33] L. M. Biga *et al.*, "Anatomy & physiology," 2020.

[34] L. Sörnmo and P. Laguna, *Bioelectrical signal processing in cardiac and neurological applications*. Academic Press, 2005.

[35] T. Giorgino, "Computing and visualizing dynamic time warping alignments in R: the dtw package," *Journal of statistical Software*, vol. 31, pp. 1-24, 2009.

[36] H. Drucker, C. J. Burges, L. Kaufman, A. Smola, and V. Vapnik, "Support vector regression machines," *Advances in neural information processing systems*, vol. 9, pp. 155-161, 1997.

[37] M. Kudo and J. Sklansky, "Comparison of algorithms that select features for pattern classifiers," *Pattern recognition*, vol. 33, no. 1, pp. 25-41, 2000.

[38] F. Pedregosa *et al.*, "Scikit-learn: Machine learning in Python," *the Journal of machine Learning research*, vol. 12, pp. 2825-2830, 2011.

[39] S. Hassan and P. Turner, "Systolic time intervals: a review of the method in the non-invasive investigation of cardiac function in health, disease and clinical pharmacology," *Postgraduate Medical Journal*, vol. 59, no. 693, pp. 423-434, 1983.

[40] A. Taebi, B. E. Solar, A. J. Bomar, R. H. Sandler, and H. A. Mansy, "Recent advances in seismocardiography," *Vibration*, vol. 2, no. 1, pp. 64-86, 2019.

[41] F. Khosrow-Khavar, K. Tavakolian, A. P. Blaber, J. M. Zanetti, R. Fazel-Rezai, and C. Menon, "Automatic annotation of seismocardiogram with high-frequency precordial accelerations," *IEEE journal of biomedical and health informatics*, vol. 19, no. 4, pp. 1428-1434, 2014.

[42] M. J. Tadi *et al.*, "A new algorithm for segmentation of cardiac quiescent phases and cardiac time intervals using seismocardiography," in *Sixth International Conference on Graphic and Image Processing (ICGIP 2014)*, 2015, vol. 9443: International Society for Optics and Photonics, p. 94432K.

[43] K. Tavakolian, B. Kaminska, A. Vaseghi, and H. Kennedy-Symonds, "Respiration analysis of the sternal ballistocardiograph signal," in *2008 Computers in Cardiology*, 2008: IEEE, pp. 401-404.

[44] M. J. Tadi *et al.*, "Gyrocardiography: A new non-invasive monitoring method for the assessment of cardiac mechanics and the estimation of hemodynamic variables," *Scientific reports*, vol. 7, no. 1, pp. 1-11, 2017.

[45] M. Di Rienzo, E. Vaini, and P. Lombardi, "An algorithm for the beat-to-beat assessment of cardiac mechanics during sleep on Earth and in microgravity from the seismocardiogram," *Scientific reports*, vol. 7, no. 1, pp. 1-12, 2017.

[46] K. Tavakolian, "Characterization and analysis of seismocardiogram for estimation of hemodynamic parameters," Applied Science: School of Engineering Science, 2010.